Geophysical Prospecting, 2007, **55**, 223–234

Non-minimum phase wavelet estimation by non-linear optimization of all-pass operators

Somanath Misra* and Mauricio D. Sacchi

Department of Physics, University of Alberta, Edmonton, Canada

Received February 2006, revision accepted September 2006

ABSTRACT

Convolution of a minimum-phase wavelet with an all-pass wavelet provides a means of varying the phase of the minimum-phase wavelet without affecting its amplitude spectrum. This observation leads to a parametrization of a mixed-phase wavelet being obtained in terms of a minimum-phase wavelet and an all-pass operator. The Wiener–Levinson algorithm allows the minimum-phase wavelet to be estimated from the data. It is known that the fourth-order cumulant preserves the phase information of the wavelet, provided that the underlying reflectivity sequence is a non-Gaussian, independent and identically distributed process. This property is used to estimate the all-pass operator from the data that have been whitened by the deconvolution of the estimated minimum-phase wavelet. Wavelet estimation based on a cumulant-matching technique is dependent on the bandwidth-to-central-frequency ratio of the data. For the cumulants to be sensitive to the phase signatures, it is imperative that the ratio of bandwidth to central frequency is at least greater than one, and preferably close to two. Pre-whitening of the data with the estimated minimum-phase wavelet helps to increase the bandwidth, resulting in a more favourable bandwidth-to-central-frequency ratio. The proposed technique makes use of this property to estimate the all-pass wavelet from the prewhitened data. The paper also compares the results obtained from both prewhitened and non-whitened data. The results show that the use of prewhitened data leads to a significant improvement in the estimation of the mixed-phase wavelet when the data are severely band-limited. The proposed algorithm was further tested on real data, followed by a test involving the introduction of a 90°-phase-rotated wavelet and then recovery of the wavelet. The test was successful.

INTRODUCTION

The process of deconvolution requires a proper estimation of the wavelet so as to obtain a more accurate estimation of the underlying reflectivity series. The reflectivity series is commonly assumed to be white, even though it is a well-known fact that it is not white in the majority of the cases (Walden and Nunn 1988; Rosa and Ulrych 1991; Saggaf and Robinson 2000). We do not attempt to address the problem of the non-white behaviour of the reflectivity series here. We make the assumption that the reflectivity series is a stationary, non-Gaussian and statistically independent random process (Walden 1985). Convolution of the reflectivity with the source wavelet makes the reflectivity series lose the high-frequency components. Deconvolution, with the assumption that the wavelet is minimum phase, removes the wavelet-amplitude signature from the data quite effectively. However, it leaves behind a spurious phase signature in the data. In order that the wavelet phase response is also effectively removed, it is necessary to deconvolve the data with an optimum mixed-phase wavelet. Classical approaches such as the Wiener–Levinson predictive deconvolution are intended to estimate the inverse minimum-phase wavelet in the data. These methods are based on second-order statistical assumptions (Robinson 1967;

*E-mail: smisra@phys.ualberta.ca

Peacock and Treitel 1969; Robinson and Treitel 1980). In other words, by assuming that the reflectivity is white, autocorrelation of the seismic trace can be used as an estimator of the autocorrelation of the wavelet. Since the autocorrelation of the wavelet does not contain phase information, an additional assumption about the wavelet is required. In general, the additional assumption is that the wavelet is minimum phase. With these two assumptions of white reflectivity and minimum-phase wavelet, it is possible to recover the seismic wavelet by measuring the autocorrelation of the trace. It is clear that if the wavelet contains non-minimum-phase components, the classical procedure outlined above is sure to fail. Fortunately, it is possible to design wavelet-estimation strategies based on higher-order statistical estimators such as the third-order and fourth-order cumulants. Unlike the autocorrelation function, which is a second-order cumulant, the third- and fourth-order cumulants do preserve the phase of the wavelet when the reflectivity consists of a non-Gaussian white process (Mendel 1991; Lazear 1993). Following Lazear (1993) and Velis and Ulrych (1996), we preferred to use the fourth-order cumulants rather than the third-order cumulants, because the third-order cumulant vanishes for symmetric distributions. Since there is no evidence that suggests that reflection coefficients should be modelled via a non-symmetric distribution, we preferred not to utilize the third-order cumulant. The fourth-order cumulants, on the other hand, do not suffer from this shortcoming.

Many different approaches have been made to bypassing the minimum-phase assumption when estimating a wavelet that shows mixed-phase character. Such methods include homomorphic deconvolution (Oppenheim *et al.* 1968; Ulrych 1971; Ulrych *et al.* 1995), minimum entropy deconvolution (Wiggins 1978), fourth-order-cumulant matching (Lazear 1993), and others.

Tugnait (1987) proposed a fourth-order-cumulant-matching technique to estimate a mixed-phase moving average wavelet. Lazear (1993) applied this technique to real seismic data. Velis and Ulrych (1996) applied the technique with a non-linear optimization approach. They estimated the mixed-phase wavelet from the fourth-order cumulant of the trace by means of the very fast simulated-annealing optimization method. They showed the dependence of the cumulant-matching technique on the ratio of bandwidth to central frequency of the data.

An improvement over the previous cumulant-matching approaches to mixed-phase deconvolution is proposed here. Parametrization of the mixed-phase wavelet as a convolution of a minimum-phase wavelet with an all-pass wavelet (Porsani and Ursin 1998; Porsani and Ursin 2000) can simplify the problem significantly. Deconvolving the seismic trace by the estimated minimum-phase wavelet helps to broaden the bandwidth of the deconvolved data. This is a desirable effect. As pointed out earlier by Velis and Ulrych (1996), a proper estimation of the mixed-phase wavelet by a cumulant-matching technique is possible when the ratio of the bandwidth to central frequency is greater than 1 and preferably close to 2. Hence, deconvolution by the estimated minimum-phase wavelet works favourably for the cumulant-matching technique. Optimization for the all-pass wavelet is performed by means of the technique of simulated annealing (Sen and Stoffa 1995). The optimization could be performed by linearizing the problem. In blind deconvolution problems like the one we are trying to solve, the topology of the cost function is unknown and it could have multiple minima. This prompted us to prefer a stochastic global-optimization approach over the linearization approach so that the problems associated with a possible multimodal cost function could be reduced.

THEORY

With the assumptions that the reflectivity series is non-Gaussian, stationary and a statistically independent random process, the fourth-order cumulant of the trace is equal to, within a scale factor, the fourth-order moment of the wavelet (Lazear 1993; Velis and Ulrych 1996; Liang, Cai and Li 2002). A further discussion about this is provided in the next section. We have already mentioned that the assumption that the reflectivity is a white process is questionable, as far as the true nature of the reflectivity series is concerned (Saggaf and Robinson 2000). However, in the present context, the above assumption is considered to be valid and the algorithm is based purely upon the validity of the white reflectivity assumption. The issue that relates to the estimation of the wavelet phase and the non-white nature of the reflectivity series is not addressed here and is considered beyond the scope of the paper. When the wavelet is parametrized as a convolution of a minimum-phase wavelet and an all-pass wavelet, the fourth-order cumulant of the whitened trace (deconvolved by the minimum-phase wavelet) is equal to, within a scale factor, the fourth-order moment of the all-pass wavelet. The cumulants and moments are discussed in the Appendix. The minimum-phase wavelet estimated from the autocorrelation of the trace has the same amplitude spectrum as that of the corresponding mixed-phase wavelet. Thus, deconvolving the trace with the minimum-phase wavelet not only removes the wavelet-amplitude spectrum from the data but also increases the bandwidth. This is a favourable result as a higher ratio of the data

bandwidth to central frequency is desired for more reliable wavelet estimation. The whitened trace now contains only the phase information of the wavelet. Hence, an all-pass wavelet remains to be optimized from the whitened data.

The seismic data can be expressed as

$$d_t = r_t * w_t, \tag{1}$$

where d_t is the seismic data, r_t is the reflectivity series and w_t is the mixed-phase wavelet. The asterisk indicates convolution between the reflectivity sequence and the wavelet. As already mentioned, w_t can be parametrized as the convolution of the minimum-phase wavelet and the all-pass wavelet (Porsani and Ursin 1998). Thus,

$$w_t = \tilde{w}_t * f_t, \tag{2}$$

where $\tilde{w}_t$ is the minimum-phase wavelet estimated from the trace and f_t is the all-pass wavelet. The Z-transform of the all-pass wavelet can be written as (Porsani and Ursin 1998)

$$F(Z) = Z^p \frac{B(Z^{-1})}{B(Z)}, \tag{3}$$

where $B(Z) = b_0 + b_1 Z + b_2 Z^2 + \cdots + b_\alpha Z^p$ and the term Z^p accounts for the time shift required to make the all-pass wavelet causal. It is important to mention here that the time series, $b_t = b_0, b_1, \ldots, b_p$, is minimum phase. This is a very simple parametrization with $b_t = b_0, b_1, \ldots, b_p$ and p as unknowns. In this problem, the term Z^p in equation (3) is not important because it only accounts for the time shift in the final estimation of the wavelet.

Substituting for w_t in equation (1), we have

$$d_t = r_t * \tilde{w}_t * f_t. \tag{4}$$

Using the Z-transform, the above equation can be represented as

$$D(Z) = R(Z)\tilde{W}(Z)F(Z). \tag{5}$$

Deconvolution by the minimum-phase wavelet yields

$$\tilde{D}(Z) = R(Z)F(Z), \tag{6}$$

where $\tilde{D}(Z)$ is the deconvolved trace that has been whitened by the removal of the minimum-phase wavelet. Thus, ideally, the reflectivity sequence can be obtained by deconvolving the whitened trace by an optimum all-pass wavelet.

Taking the Z-transform of both sides of equation (2), we obtain

$$W(Z) = \tilde{W}(Z)F(Z). \tag{7}$$

This can be written as

$$|W(Z)|e^{i\theta(Z)} = \left|\tilde{W}(Z)\right|e^{i\theta_{\min}(Z)}\left|F(Z)\right|e^{i\theta_F(Z)}, \tag{8}$$

where $|W(Z)|$ is the amplitude spectrum of the mixed-phase wavelet, $|\tilde{W}(Z)|$ is the amplitude spectrum of the estimated minimum-phase wavelet and $|F(Z)|$ is the amplitude spectrum of the all-pass wavelet, which is equal to 1. Also, $\theta(Z)$ is the phase of the mixed-phase wavelet, $\theta_{\min}(Z)$ is the phase of the minimum-phase wavelet and $\theta_F(Z)$ is the phase of the all-pass wavelet. Since $|W(Z)| = |\tilde{W}(Z)|$, we have

$$\theta(Z) = \theta_{\min}(Z) + \theta_F(Z). \tag{9}$$

The problem of estimating the mixed-phase wavelet can now be posed as a problem of estimating the optimum phase of the all-pass wavelet from the data whitened by an estimated minimum-phase wavelet. Whitening the data by an estimated minimum-phase wavelet has a trade-off in terms of offering a wider bandwidth and enhanced noise level. It is observed that, in general, the practice of whitening deconvolution helps to enhance the bandwidth in a frequency zone where the signal is stronger than the noise. In the problems of wavelet-phase estimation, the accuracy of the estimated phase depends, to a large extent, on the bandwidth of the data. Any amount of enhanced bandwidth in a frequency zone where the signal is stronger than the noise would greatly help in the phase estimation of the wavelet. Even though prewhitening of the data does not introduce any new information into the data, it certainly helps in shaping the data in such a way that the phase estimation is performed in a more conducive data environment (White 1988, pers. comm.; White and Simm 2003).

DEVELOPMENT OF THE ALGORITHM

The phase estimation by the cumulant-matching technique is performed using the simulated-annealing algorithm, which is a non-linear stochastic optimization tool. Simulated annealing has been applied quite successfully in many geophysical inversion problems. Many variants of the simulated-annealing technique, such as the Metropolis algorithm (Metropolis *et al*. 1953; Kirkpatrick *et al*. 1983), the heat bath algorithm (Creutz 1984; Geeman and Geeman 1984; Rebbi 1984; Rothman 1986), simulated annealing (Greene and Supowit 1986), fast simulated annealing (Szu and Hartley 1987), very fast simulated annealing (Ingber 1989) and mean field annealing (Peterson and Anderson 1987, 1988; Peterson and Soderberg 1989) have been developed with wide and successful applications.

We used the Metropolis algorithm to optimize for the model parameters b_t, the Z-transform of which forms the denominator of the all-pass wavelet (equation 3). The unknowns here are the length of $b_t(p)$ and its coefficients. The optimization is performed by fixing p at a value of 4. This is the minimum length of b_t that can produce a combination of real and imaginary roots in the Z-plane. It is also noted that b_t is minimum phase in character. A minimum-phase sequence is obtained by the Kolmogoroff technique (Claerbout 1992) applied to a randomly generated sequence. The cost function for the optimization is obtained from the Bartlett–Brillinger–Rosenblatt formula (Mendel 1991; Lazear 1993). The formula is given by the following convolutional equation:

$$C_4^{\mathrm{s}}(\tau_1, \tau_2, \tau_3) = C_4^{\mathrm{r}}(\tau_1, \tau_2, \tau_3) * M_4^{\mathrm{w}}(\tau_1, \tau_2, \tau_3) + C_4^{\mathrm{v}}(\tau_1, \tau_2, \tau_3), \tag{10}$$

where $C_4^{\mathrm{s}}(\tau_1, \tau_2, \tau_3)$ is the fourth-order cumulant of the seismic trace, $C_4^{\mathrm{r}}(\tau_1, \tau_2, \tau_3)$ is the fourth-order cumulant of a non-Gaussian, statistically independent and identically distributed reflectivity sequence, $M_4^{\mathrm{w}}(\tau_1, \tau_2, \tau_3)$ is the fourth-order moment of the wavelet and $C_4^{\mathrm{v}}(\tau_1, \tau_2, \tau_3)$ is the fourth-order cumulant of a Gaussian additive noise. The lags are represented by τ_1, τ_2 and τ_3. Under the assumption that there exist an infinite number of data, along with the other assumptions about the reflectivity sequence mentioned previously, the term $C_4^{\mathrm{r}}(\tau_1, \tau_2, \tau_3)$ reduces to an impulse at the central lag, scaled by the kurtosis (γ^{r}) of the reflectivity series. The term $C_4^{\mathrm{v}}(\tau_1, \tau_2, \tau_3)$ involving the Gaussian noise reduces to zero. Hence, under the above assumptions, equation (10) becomes

$$C_4^{\mathrm{s}}(\tau_1, \tau_2, \tau_3) = \gamma^{\mathrm{r}} M_4^{\mathrm{w}}(\tau_1, \tau_2, \tau_3), \tag{11}$$

where γ^{r} is the kurtosis of the reflectivity sequence which is a constant. γ^r is zero for a purely Gaussian reflectivity series (Lazear 1993).

Thus, the cost function for the optimization is given by

$$J = \sum_{\tau_1} \sum_{\tau_2} \sum_{\tau_3} \left[\tilde{C}_4^{\mathrm{s}}(\tau_1, \tau_2, \tau_3) - \tilde{M}_4^{\mathrm{w}}(\tau_1, \tau_2, \tau_3) \right]^2, \tag{12}$$

where $\tilde{C}_4^{\mathrm{s}}(\tau_1, \tau_2, \tau_3)$ is the fourth-order trace cumulant (normalized by the central lag cumulant) and $\tilde{M}_4^{\mathrm{w}}(\tau_1, \tau_2, \tau_3)$ is the fourth-order wavelet moment (normalized by the central lag moment). A detailed explanation of the cost function is provided in the Appendix. Figs 1(a,b) shows the flowcharts for the estimation of the mixed-phase wavelet from the whitened data.

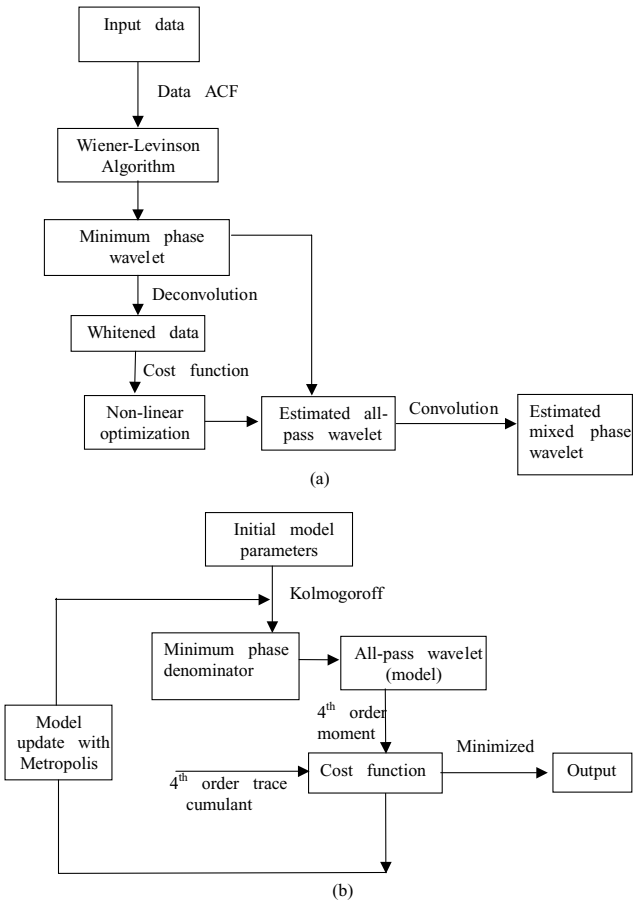

Figure 1 The flowcharts. (a) Flowchart for the estimation of the mixed-phase wavelet. (b) Flowchart for the non-linear optimization of the all-pass operators.

SYNTHETIC DATA EXAMPLE

The proposed algorithm for estimating the mixed-phase wavelet is tested by designing a synthetic mixed-phase wavelet and a synthetic trace. Table 1 shows the roots of the Z-transform of the wavelet coefficients that are considered to generate the synthetic mixed-phase wavelet. A similar wavelet was used by Porsani and Ursin (2000) to test their algorithm.

Fig. 2(a) shows the synthetic trace. The synthetic trace was generated by convolving a Laplacian mixture distribution of reflectivity sequence (number of data points $N = 250$) with the true mixed-phase wavelet. This particular distribution of the reflectivity series is chosen so as to obtain a better approximation of the true reflectivity distribution (Walden and Hosken 1986). The Laplacian mixture distribution was obtained by generating two separate Laplacian random deviates

Table 1 The roots of the synthetic wavelet. Negative phase angles indicate the complex conjugate of the corresponding roots

No.	1	2	3	4	5	6	7	8	9
Magnitude	1/1.3	1/1.5	1/1.11	1.2	1.3	1.8	1.95	1.25	1.8
Phase (degree)	0	0	+45	+5	+60	0	180	+120	+160
			−45	−5	−60			−120	−160

and mixing them together by means of a mixing parameter. The first Laplacian deviate was generated using a Laplace parameter (σ_1) equal to 0.007. The second Laplacian deviate was generated using a Laplace parameter (σ_2) equal to 0.017. The mixing parameter in our case was chosen to be 23% of the deviates generated by the smaller Laplace parameter. The trace does not contain any noise component. Fig. 2(b) shows the data after deconvolution with the estimated minimum-phase wavelet. The whitened data obtained in this way have a larger bandwidth compared to the original data and contain only the phase information of the wavelet as the amplitude information has been effectively removed by the deconvolution. Hence, the technique of cumulant matching reduces to the matching of the fourth-order moment of the all-pass wavelet and the fourth-order cumulant of the whitened data. Fig. 2(c) shows the true mixed-phase wavelet. Fig. 2(d) shows the estimated minimum-phase wavelet obtained from the data by the Wiener–Levinson algorithm. Fig. 2(e) shows the estimated mixed-phase wavelet for a model length $p = 4$. The correlation measure between the true wavelet and the estimated mixed wavelet is 0.99.

Comparison of results

A comparison is called for between the estimation of the mixed-phase wavelet using the proposed algorithm and that obtained directly from the data. The cumulant-matching technique is not sensitive when the data bandwidth-to-central-frequency ratio is less than 1. Hence, it is expected that the cumulant-matching technique will not be able to perform well when the mixed-phase wavelet is estimated from severely band-limited data that have a ratio of bandwidth to central frequency of less than 1. The proposed technique has the advantage of removing the wavelet-amplitude spectrum from the data, thus resulting in a wider bandwidth of the whitened data within a frequency zone where the signal is stronger than the noise. This allows the cumulant-matching technique to be carried out in a favourable domain and hence the result is expected to be better.

A mixed-phase wavelet with a bandwidth-to-central-frequency ratio of 0.5 was chosen for the purpose of illustration. Fig. 3(a) shows the synthetic trace that was generated by convolving a band-limited wavelet with a reflectivity series of length $N = 250$. The reflectivity series has a Laplacian mixture distribution generated by the same parameters mentioned above. The synthetic trace does not have any noise component. Fig. 3(b) shows the whitened data after deconvolving the data with the estimated minimum-phase wavelet; Fig. 3(c) shows the true band-limited wavelet with the bandwidth-to-central-frequency ratio equal to 0.5; Fig. 3(d) shows the corresponding minimum-phase wavelet estimated from the data. Fig. 4(a) shows the estimated mixed-phase wavelet for a model length $p = 4$. The estimation is performed over a whitened trace that is obtained by deconvolving the trace with the estimated minimum-phase wavelet. The correlation measure between the estimated wavelet and the true wavelet is calculated to be 0.99. The algorithm was further applied to the same data and the mixed-phase wavelet was estimated without deconvolving the trace with the estimated minimum-phase wavelet. Fig. 4(b) shows the estimated mixed-phase wavelet obtained from the non-whitened data. The correlation measure obtained for this estimation was found to be 0.89, which is much lower than with the estimated wavelet obtained from the whitened data.

In order to substantiate the above test further, we conducted 200 Monte-Carlo simulations with different realizations of the synthetic data for different numbers of data points. We used a zero-phase band-limited Ricker wavelet (central frequency = 30 Hz, time sample interval = 0.004 s) in our simulations. The simulations for estimations from whitened and non-whitened data were performed for the numbers of data points, $N = 250$ and $N = 500$. Fig. 5(a) shows the correlation measures between the estimated and the true wavelets for both prewhitened and non-whitened data. The dashed line represents the estimation from non-whitened data and the

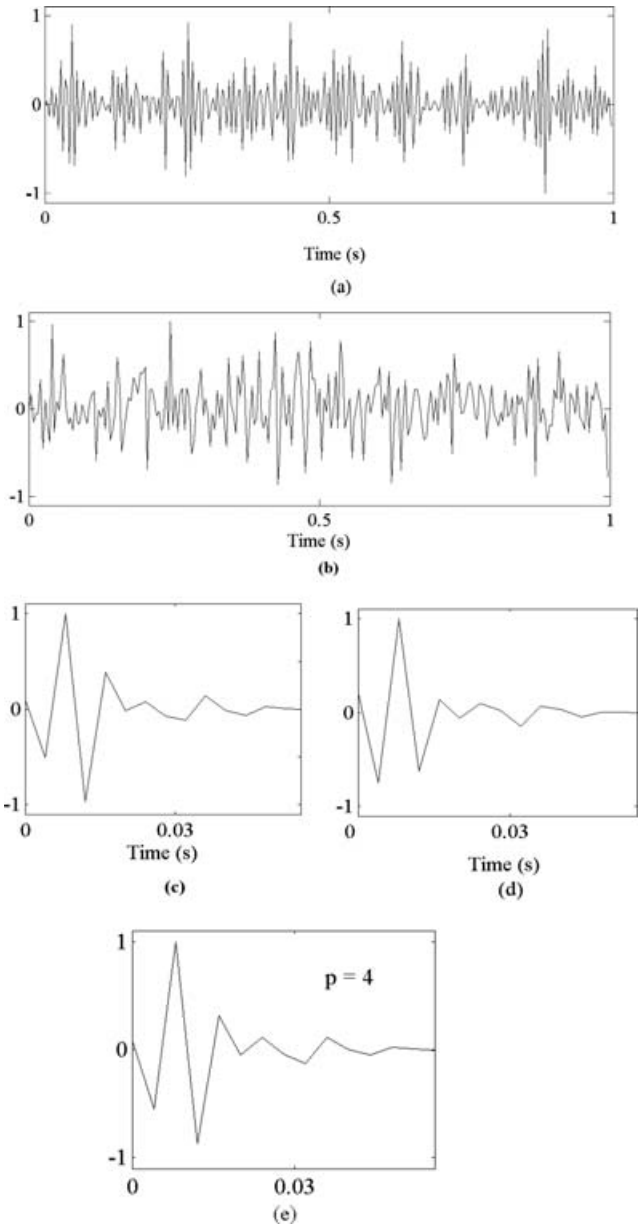

Figure 2 (a) The synthetic data. (b) The data whitened by deconvolution with the estimated minimum-phase wavelet. (c) The true synthetic wavelet. (d) The estimated minimum-phase wavelet. (e) The estimated mixed-phase wavelet for a model length $p = 4$. The estimated wavelet has a correlation measure of 0.99 with the true wavelet. Number of data points $N = 250$.

solid line represents the estimation from the prewhitened data. Fig. 5(b) shows the error bars for the root-mean-square (rms) error between the estimated and the true wavelets for 200 simulations for $N = 250$. Fig. 5(c) shows the correlation between the estimated and the true wavelets for 200

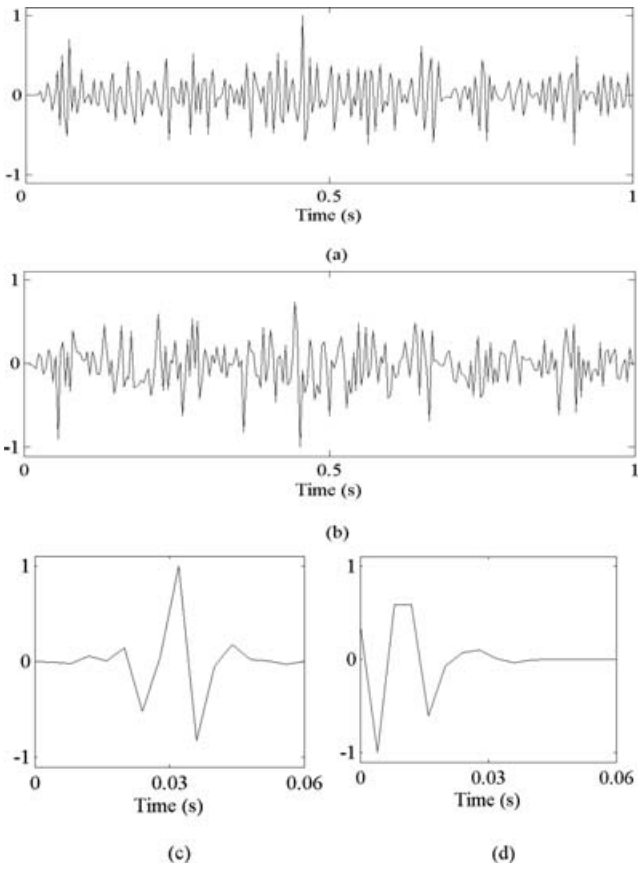

Figure 3 (a) The synthetic data. (b) The data whitened by deconvolution with the estimated minimum-phase wavelet. (c) The true mixed-phase wavelet with a bandwidth-to-central-frequency ratio of 0.5. (d) The estimated minimum-phase wavelet. Number of data points $N = 250$.

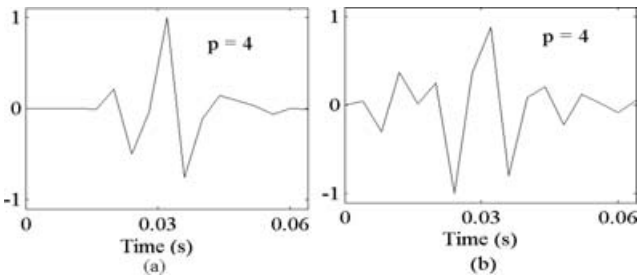

Figure 4 Mixed-phase wavelet estimation from the whitened and non-whitened data. (a) The estimated mixed-phase wavelet from the prewhitened data. Model length $p = 4$. The correlation with the true wavelet (Fig. 3c) is 0.99. (b) The estimated mixed-phase wavelet from non-whitened data for model length $p = 4$. The correlation of the estimated wavelet with the true wavelet is 0.89. Number of data points $N = 250$.

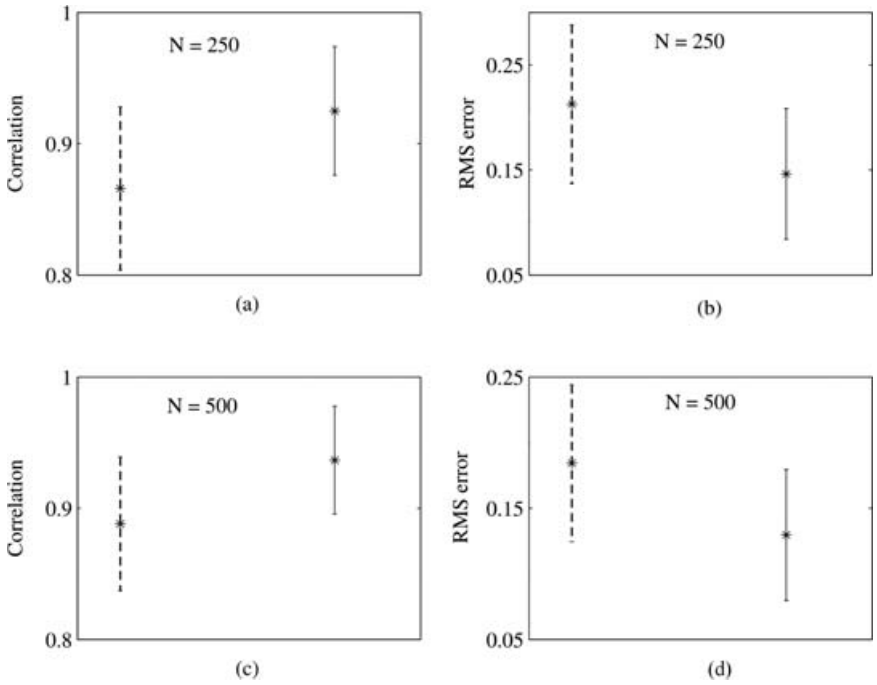

Figure 5 Comparison between the estimations from prewhitened and non-whitened data. N is number of data points considered for estimation. The dashed line represents the estimations from non-whitened data and the solid line represents the estimations from the prewhitened data. (a) The correlation measure between the estimated and true wavelets for $N = 250$. (b) The rms error between the estimated and the true wavelets for $N = 250$. (c) The correlation measure between the estimated and true wavelets for $N = 500$. (d) The rms error between the estimated and the true wavelets for $N = 500$. 200 Monte-Carlo simulations were used.

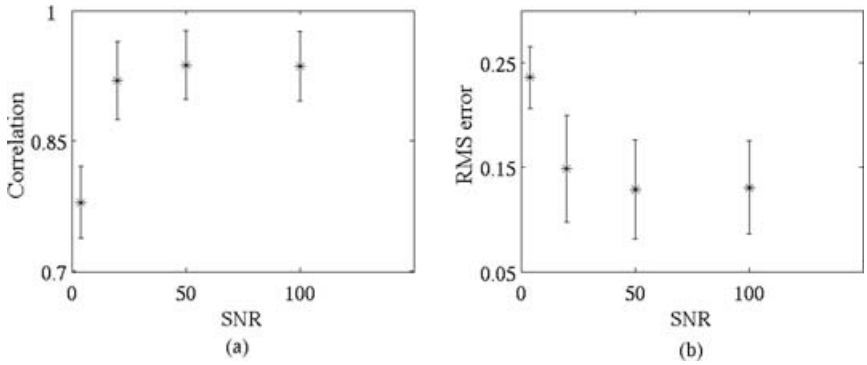

Figure 6 Test of the stability of the algorithm with different signal-to-noise ratios. (a) The correlation measure plotted against *SNR*. (b) The rms error plotted against *SNR*. *SNR* = [4, 20, 50, 100]. 200 Monte-Carlo simulations were used.

simulations with $N = 500$. Fig. 5(d) shows rms error between the estimated and true wavelets for $N = 500$. It can be seen that the mean correlation is high with low variance when the estimation is performed over prewhitened data as compared to that when the estimation is performed with the non-whitened data. It can also be observed that the rms error is low with smaller variance when the estimation is carried out with the prewhitened data.

These observations corroborate the fact that the cumulant-matching technique is sensitive to the ratio of the bandwidth to central frequency. A better estimation of the wavelet was obtained because this ratio could be improved by whitening the trace with the estimated minimum-phase wavelet.

Effect of noise and number of data points

The algorithm was tested with different levels of noise in the synthetic data. The data were synthetically generated by convolving a zero-phase Ricker wavelet (central frequency =

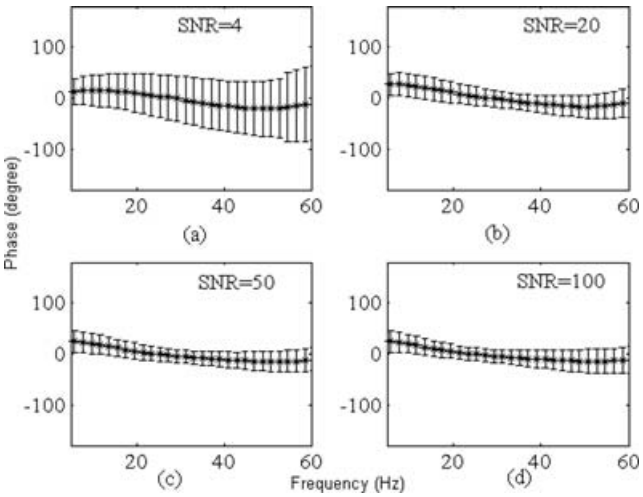

Figure 7 The error bars for the de-trended phase spectrum of the estimated wavelet for different noise levels in the data, defined in terms of the signal-to-noise ratio. (a) $SNR = 4$. (b) $SNR = 20$. (c) $SNR = 50$. (d) $SNR = 100$. Number of data points $N = 500$. 200 Monte-Carlo simulations were used.

30 Hz and sampling interval = 0.004 s) with a randomly generated reflectivity sequence that followed a Laplacian mixture distribution. The distribution of the data was obtained using the Laplace parameters and the mixing parameter mentioned above. The test was carried out over 500 data samples. A total of 200 Monte-Carlo simulations were performed for each noise level defined in terms of the signal-to-noise ratio (SNR), given by the following equation:

$$SNR = \frac{\max |d|}{\sigma}, \tag{13}$$

where d is the data and s is the standard deviation of the noise. The following signal-to-noise ratio values, $SNR = [4, 20, 50, 100]$ were considered in order to test the stability of the algorithm.

Fig. 6(a) shows the error bars for the correlation measure between the true wavelet and the estimated wavelet. As anticipated, the correlation measure between the true wavelet and the estimated wavelet shows an increase as *SNR* is increased from 4 to 20, and it then remains almost constant as the algorithm enters into a more stable regime of the SNR. Fig. 6(b) shows the rms error plotted against *SNR*. The rms error between the true wavelet and the estimated wavelet decreases as *SNR* is increased from 4 to 20 and it then remains almost constant. The constant region indicates that the algorithm is operating in a more stable regime of the SNR. There exists a trade-off between the degree of prewhitening and the enhancement of noise (White 1984, 1988; White and Simm 2003). The Monte-Carlo simulations show that the algorithm operates in a more stable domain when *SNR* is close to 20 and above. Fig. 7 shows the phase spectrum of the estimated wavelet for the 200 Monte-Carlo simulations. The phase spectrum has been de-trended to remove the linear trend in the phase that was introduced by the constant time shift. Since the true wavelet is zero-phase, it is expected that the recovered phase (after de-trending) should be close to zero for all frequencies. We considered 200 Monte-Carlo simulations for a total of 500 data points with a signal-to-noise ratio, SNR = [4, 20, 50, 100]. Figs 7(a.b.c.d) shows the error bars for the de-trended phase spectra for $SNR = 4, 20, 50, 100$, respectively. It can be seen that as *SNR* increases, the accuracy in the phase estimation also increases.

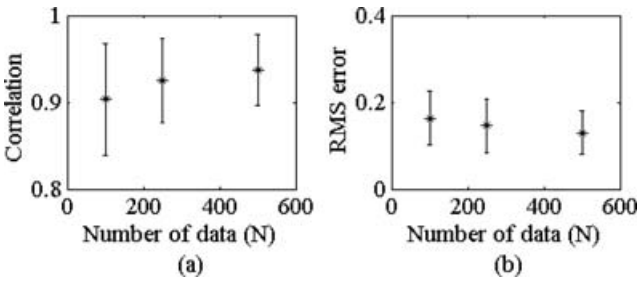

Figure 8 Test of the stability of the algorithm with different numbers of data. (a) The correlation measure plotted against the number of data. (b) The rms error plotted against the number of data. $SNR = 40$. 200 Monte-Carlo simulations were used.

It is known that the statistical methods of wavelet estimation depend significantly on the data volume. As discussed previously, the cost function (equation 12) is obtained under the assumption (along with the assumptions about the statistical properties of the reflectivity sequence) that an infinite number of data exist. This makes it necessary to run the proposed algorithm on varying numbers of data so as to obtain a measure of the stability of the algorithm. The following numbers of data points, $N = [100, 250, 500]$, were considered in order to test the algorithm.

A total of 200 Monte-Carlo simulations were performed for a given number of data points. *SNR* was kept fixed at 40 during all the simulations. Fig. 8(a) shows the correlation measure for different numbers of data points. As anticipated, the correlation measure between the true wavelet and the estimated wavelet increased as the number of data points increased from 100 to 250 and then to 500. Fig. 8(b) shows the rms error plotted against the number of data points. The rms error is calculated between the true wavelet and the

estimated wavelet and it decreases as the number of data points is increased. It appears that for all practical purposes, with a reasonable number of data points, the algorithm is capable of estimating the wavelet with reasonable accuracy.

The estimation of the wavelet from a given set of data is also dependent on the non-stationarity issues involving the wavelet. However, in the present context, it is assumed that the wavelet is stationary in both spatial and temporal axes, and the non-stationarity issues are considered beyond the scope of the paper.

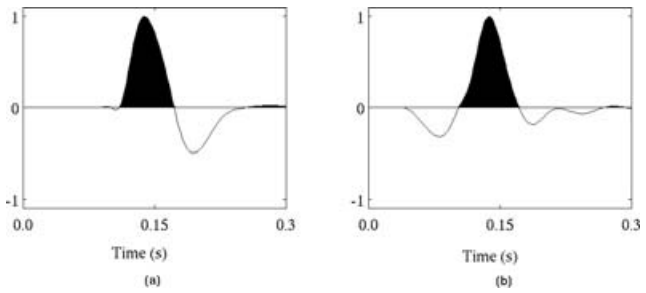

Figure 9 (a) The estimated minimum-phase wavelet obtained from the real data. (b) The estimated mixed-phase wavelet.

REAL DATA EXAMPLE

A stacked seismic section was considered for testing the algorithm. Seismic data with 77 traces and 200 time samples were windowed from the stacked section. The average cumulant was calculated for the data window and incorporated in the cost function (equation 12) for the estimation of the all-pass operator. An average minimum-phase wavelet was estimated from the data using the Wiener–Levinson algorithm. The data were prewhitened by deconvolving them with the estimated minimum-phase wavelet.

Fig. 9(a) shows the estimated minimum-phase wavelet obtained from the data using the Wiener–Levinson algorithm and Fig. 9(b) shows the estimated mixed-phase wavelet obtained from the data with the proposed algorithm. Fig. 10(a) shows the true stacked section; Fig. 10(b) shows the section after deconvolution with the estimated minimum-phase wavelet; Fig. 10(c) shows the dephased stacked section after subtracting the phase of the estimated all-pass operator from the minimum-phase deconvolved data shown in Fig. 10(b). The algorithm was test run on a real data set that shows less interference between the reflection events. This data set provided the preliminary information about the type of wavelet that is present in the data. Fig. 10(a) shows a reflection event positioned approximately midway between 0 s

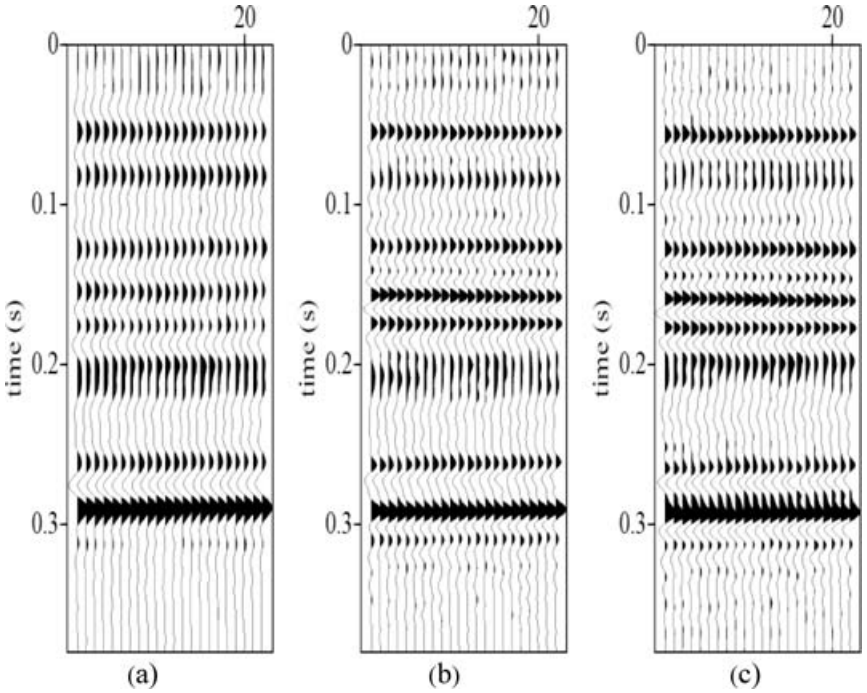

Figure 10 Real data example. (a) A window of the data. (b) Minimum-phase deconvolution of the data. (c) Mixed-phase deconvolution of the data. The result of the minimum-phase deconvolution is illustrated here for comparison with the result obtained from the mixed-phase deconvolution. The average fourth-order cumulant is calculated over 77 traces and 200 time samples.

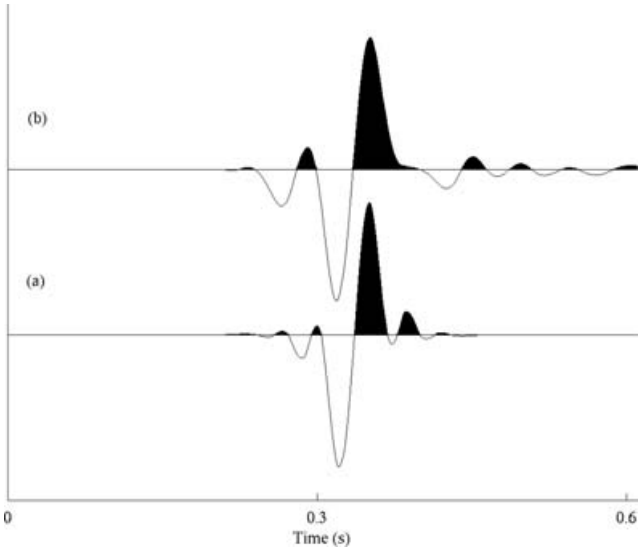

Figure 11 (a) The true 90°-constant-phase-rotated wavelet. (b) The recovered wavelet.

and 0.1 s (the first coherent event in the seismic section) on the time axis. This event is fairly isolated and does not indicate any large degree of interference from the nearby reflection events. It provides an indication about the type of wavelet that is present in the data. The algorithm was able to estimate a wavelet from the data that resembled the preliminary information obtained from the isolated reflection event. In order to test the algorithm, the deconvolved data were further convolved with a 90°-constant-phase-rotated synthetic wavelet. The algorithm was applied to this data to check if the new phase-rotated wavelet could be effectively recovered (Hargreaves 1994). Fig. 11(a) shows the true synthetic 90°-phase-rotated wavelet. Fig. 11(b) shows the wavelet recovered by the proposed algorithm. It can be seen that the algorithm was able to estimate the convolved wavelet effectively.

CONCLUSIONS

Deconvolution with the estimated minimum-phase wavelet results in enhancing the bandwidth of the deconvolved data. Since the mixed-phase wavelet and its corresponding minimum-phase wavelet have the same amplitude spectrum, deconvolution with the minimum-phase wavelet effectively removes the amplitude spectrum of the wavelet. This leaves the data that require only a phase correction. The required phase correction is attainable by means of a simple and short parametrization of the mixed-phase wavelet. This is the main advantage of the proposed algorithm. The optimization algorithm involves the matching of the fourth-order cumulant of the whitened data with the fourth-order moment of the all-pass operator. The cumulant-matching technique works well when the bandwidth-to-central-frequency ratio of the data is greater than 1. The technique is most suitable when this ratio is close to 2, i.e. the data is full band. The proposed technique separates the minimum-phase part of the wavelet from the data by deconvolving the data with an estimated minimum-phase wavelet. As a result, the deconvolved data contain only the phase signature of the mixed-phase wavelet. This also allows the cumulant-matching technique to work in a favourable regime of the bandwidth-to-central-frequency ratio. The synthetic examples showed that the Metropolis algorithm can be used quite effectively to estimate the all-pass wavelet and hence the mixed-phase wavelet. A comparison between the wavelet estimated from the whitened data and the wavelet estimated from the non-whitened data when the wavelet was severely band-limited was also presented. The proposed algorithm allows for whitening the data using the estimated minimum-phase wavelet obtained by the Wiener–Levinson algorithm. It can be observed that when the data were band-limited, there was relatively poor correlation between the estimated mixed-phase wavelet and the true wavelet. However, suitable parametrization of the wavelet and subsequent whitening of the data improved the estimation of the mixed-phase wavelet. This is an encouraging result for the proposed algorithm. The algorithm was also tested on real data. The estimated mixed-phase wavelet from the real data compared well with the isolated reflection event, which is a good indicator of the wavelet present in the data. The test carried out by artificially convolving a 90°-phase-rotated wavelet and subsequently recovering it, was also successful.

ACKNOWLEDGEMENTS

We acknowledge Drs Neil D. Hargreaves, Milton Porsani, Danilo R. Velis and R.E. White for sharing their insightful thoughts on wavelet estimation.

REFERENCES

Claerbout J.F. 1992. *Earth Sounding Analysis. Processing Versus Inversion*. Blackwell Scientific Publications.

Creutz M. 1984. *Quarks, Gluons and Lattices*. Cambridge University Press.

Geeman S. and Geeman D. 1984. Stochastic relaxation, Gibbs' distribution and Bayesian restoration of images. *IEEE Transactions on Pattern Analysis and Machine Intelligence* PAMI-6, 721–741.

Greene J.W. and Supowit K.J. 1986. Simulated annealing without rejected moves. *IEEE Transactions on Computer-Aided Design CAD-5* **1**, 221–228.

Hargreaves N. 1994. Wavelet estimation via fourth-order cumulants. 64th SEG Meeting, Los Angeles, USA, Expanded Abstracts, 1588–1590.

Ingber L. 1989. Very fast simulated reannealing. *Mathematical and Computer Modeling* **12** (8), 967–993.

Kirkpatrick S., Delatt C.D. Jr and Vecchi M.P. 1983. Optimization by simulated annealing. *Science* **220**, 671–680.

Lazear G.D. 1993. Mixed-phase wavelet estimation using fourth-order cumulants. *Geophysics* **58**, 1042–1051.

Liang G., Cai X. and Li Q. 2002. Using high-order cumulants to extrapolate spatially variant seismic wavelets. *Geophysics* **67**, 1869–1876.

Mendel J.M. 1991. Tutorial on higher-order statistics (spectra) in signal processing and system theory: theoretical results and some applications. *Proceedings of the IEEE* **79**, 278–305.

Metropolis N., Rosenbluth A., Rosenbluth M., Teller A. and Teller E. 1953. Equation of state calculations by fast computing machines. *Journal of Chemical Physics* **21**, 1087–1092.

Oppenheim A.V., Schafer R.W. and Stockham T.G. 1968. Nonlinear filtering of multiplied and convolved signals. *Proceedings of the IEEE* **65**, 1264–1291.

Peacock K.L. and Treitel S. 1969. Predictive deconvolution: Theory and practice. *Geophysics* **34**, 155–169.

Peterson C. and Anderson J.R. 1987. A mean field theory learning algorithm for neural networks. *Complex Systems* **1**, 995–1019.

Peterson C. and Anderson J.R. 1988. Neural networks and NP-complete optimization problems; A performance study on the graph bisection problem. *Complex Systems* **2**, 59–89.

Peterson C. and Soderberg B. 1989. A new method for mapping optimization problems onto neural networks. *International Journal of Neural Sciences* **1**, 3–22.

Porsani M.J. and Ursin B. 1998. Mixed phase deconvolution. *Geophysics* **63**, 637–647.

Porsani M.J. and Ursin B. 2000. Estimation of an optimal mixed phase inverse filter. *Geophysical Prospecting* **48**, 663–676.

Rebbi C. 1984. *Monte Carlo Calculations in Lattice Gauge Theories. Applications of the Monte Carlo Method*, pp. 277–298. Springer Verlag, Inc.

Robinson E.A. 1967. Predictive deconvolution of time series with application to seismic exploration. *Geophysics* **32**, 418–484.

Robinson E.A. and Treitel S. 1980. *Geophysical Signal Analysis*. Prentice Hall, Inc.

Rosa A.L.R. and Ulrych T.J. 1991. Processing via spectral modelling. *Geophysics* **56**, 1244–1251.

Rothman D.H. 1986. Automatic estimation of large residual static corrections. *Geophysics* **51**, 337–346.

Saggaf M.M. and Robinson E.A. 2000. A unified framework for the deconvolution of traces of nonwhite reflectivity. *Geophysics* **65**, 1660–1676.

Sen M. and Stoffa P.L. 1995. *Global Optimization Methods in Geophysical Inversion*. Elsevier. Science Publishing Co.

Szu H. and Hartley R. 1987. Fast simulated annealing. *Physics Letters A.* **122**, 157–162.

Tugnait J.K. 1987. Identification of linear stochastic systems via second- and fourth-order cumulant matching. *IEEE Transactions on Information Theory* IT-33, 393–407.

Ulrych T.J. 1971. Application of homomorphic deconvolution to seismology. *Geophysics* **36**, 650–660.

Ulrych T.J., Velis R.D. and Sacchi M.D. 1995. Wavelet estimation revisited. *The Leading Edge* **14**, 1139–1143.

Velis D.R. and Ulrych T.J. 1996. Simulated annealing wavelet estimation via fourth-order cumulant matching. *Geophysics* **61**, 1939–1948.

Walden A.T. 1985. Non-Gaussian reflectivity, entropy, and deconvolution. *Geophysics* **50**, 2862–2888.

Walden A.T. and Hosken J.W.J. 1986. The nature of non-Gaussianity of primary reflection coefficients and its significance for deconvolution. *Geophysical Prospecting* **34**, 1038–1066.

Walden A.T. and Nunn K.R. 1988. Correcting for coloured primary reflectivity in deconvolution. *Geophysical Prospecting* **36**, 282–297.

White R.E. 1984. Signal and noise estimation from seismic reflection data using spectral coherence methods. *Proceedings of the IEEE* **72**, 1340–1356.

White R.E. 1988. Maximum kurtosis phase correction. *Geophysical Journal* **95**, 371–389.

White R.E. and Simm R. 2003. The importance of bandwidth in seismic cross-equalization- well tie and other examples. 65th EAGE Conference, Stavanger, Norway, Extended Abstracts, P071.

Wiggins R.A. 1978. Minimum entropy deconvolution. *Geoexploration* **16**, 21–35.

APPENDIX

The estimation of the pth-order moment of a real, stationary and discrete time series $s(n)$ is defined as

$$M_p^{\mathrm{s}}(\tau_1, \tau_2, \ldots, \tau_{p-1}) = \frac{1}{N}\sum_n s(n)s(n+\tau_1)s(n+\tau_2)\ldots s(n+\tau_{p-1}), \quad \text{(A1)}$$

where τ_1, τ_2 ... are the lags and N is the length of the time series $s(n)$.

The pth-order cumulant of the above time series is defined as

$$C_p^{\mathrm{s}}(\tau_1, \tau_2, \ldots, \tau_{p-1}) = M_p^{\mathrm{s}}(\tau_1, \tau_2, \ldots, \tau_{p-1}) - M_p^{\mathrm{G}}(\tau_1, \tau_2, \ldots, \tau_{p-1}), \quad \text{(A2)}$$

where M_p^{G} is the moment of an equivalent Gaussian time series having the same mean and autocorrelation as that of s(n) (Mendel 1991).

For $p = 4$ and a zero-mean time series $s(n)$,

$$M_4^{\mathrm{G}}(\tau_1, \tau_2, \tau_3) = M_2^{\mathrm{s}}(\tau_1)M_2^{\mathrm{s}}(\tau_3 - \tau_2) + M_2^{\mathrm{s}}(\tau_2)M_2^{\mathrm{s}}(\tau_3 - \tau_1) + M_2^{\mathrm{s}}(\tau_3)M_2^{\mathrm{s}}(\tau_2 - \tau_1). \quad \text{(A3)}$$

Thus, combining equation. (A1), (A2) and (A3), we obtain the expression for the estimation of the fourth-order cumulant of

the time series $s(n)$:

$$C_4^s(\tau_1, \tau_2, \tau_3) = \frac{1}{N}\sum_n s(n)s(n+\tau_1)s(n+\tau_2)s(n+\tau_3) - \left[M_2^s(\tau_1)M_2^s(\tau_3-\tau_2) + M_2^s(\tau_2)M_2^s(\tau_3-\tau_1) + M_2^s(\tau_3)M_2^s(\tau_2-\tau_1)\right]. \quad \text{(A4)}$$

When the mean of s(n) is zero, the second- and third-order moments are equal to the respective cumulants (Mendel 1991; Lazear 1993).

The cost function, defined in equation (10), uses the normalized fourth-order cumulant of the trace, defined as

$$\tilde{C}_4^s(\tau_1, \tau_2, \tau_3) = \frac{C_4^s(\tau_1, \tau_2, \tau_3)}{C_4^s(0, 0, 0)}, \quad \text{(A5)}$$

and the normalized fourth-order moment of the wavelet, defined as

$$\tilde{M}_4^w(\tau_1, \tau_2, \tau_3) = \frac{M_4^w(\tau_1, \tau_2, \tau_3)}{M_4^w(0, 0, 0)}. \quad \text{(A6)}$$